Inline Combline Filters of Order N With up to N+1 Transmission Zeros

José Joaquín Vague, David Rubio, Miguel Angel Fuentes, Santiago Cogollos, *member, IEEE,* Mariano Baquero, *member, IEEE,* Vicente E. Boria, *Fellow, IEEE,*, and Marco Guglielmi, *Life Fellow, IEEE*

***Abstract*—In this paper we describe several alternative inline implementations for combline filters with transmission zeros located both below and above the pass-band. A systematic design procedure is also presented using a lumped-element equivalent circuit. Following the design procedure that we propose, up to N+1 transmission zeros can be implemented with an inline filter of order N. The generation of the transmission zeros is explained physically in terms of mixed inductive and capacitive couplings. Several filters are also manufactured and tested. Good agreement between measured and simulated results is demonstrated thereby fully validating the new filter concepts.**

***Index Terms*—Combline filters, high selectivity, mixed couplings, transmission zeros.**

I. Introduction

COMBLINE filters are widely used in satellite and mobile applications operating in the L- and S-band because they are compact structures, able to implement advanced responses with moderate-to-low insertion losses (IL), and with good power-handling capability [1]. The classical combline implementation in planar technology (i.e. stripline or microstrip) are based on Transversal Electro-Magnetic (TEM) resonators short-circuited at one end and loaded with a capacitor at the other end [2]. The capacitive loading allows to reduce the resonator length below a quarter-wavelength. In the first structures reported, the input and output couplings were implemented with magnetic loops (transformers), but soon after solutions based on direct tapped lines were also proposed [3]. Planar combline filters can now be considered a mature technology, with many different design techniques available in the technical literature ([4] - [10]). The planar combline filter concept has also been translated into waveguide technology, where the resonators are implemented with a cylindrical metallic post of circular cross-section with a rectangular or circular enclosure, thus resulting in a coaxial cavity implementation (see [11] - [12]). The possibility of increasing the selectivity and the out-of-band rejection of band pass filters by implementing transmission zeros (TZs) in their response is a technique that has been proposed by many researchers, in many different kinds of filters. It is, in fact, well-known that TZs can be created by introducing cross-couplings between non-adjacent cavities or resonators [13]. This technique has indeed been used in combline filters for implementing triplets [14] and quadruplets [15], or structures with source-load coupling [16]. However, the traditional implementation of this concept is based on folded structures that can have a significant footprint. To address this problem, other solutions for generating transmission zeros with inline topologies have also been proposed, using for instance the extracted pole technique [17], or using non-resonant nodes [18], [19]. In this context, one of the first solutions for introducing one or two TZs in classical inline comb filters has been proposed in [20], where the first and last resonators of the structure are used to implement TZs. Recently, the practical implementation of triplets and quadruplets in coaxial cavity (combline) filters, has been successfully demonstrated by changing the orientation of successive resonators, and preserving an inline configuration [21], [22]. Furthermore, other solutions have been also proposed for introducing TZs using mixed inter resonator coupling elements (of inductive and capacitive nature). In [23], for instance, mixed (resonant) inter resonator couplings are implemented with a suspended metallic strip, providing capacitive coupling between the open end of adjacent resonators, and a conducting pin connecting the base of the two adjacent resonators to provide an inductive coupling. A different realization of the mixed coupling, based on series lumped capacitors in parallel with the series inductance of evanescent-mode waveguide sections, is shown in [24], leading to compact inline pseudo-elliptic evanescent-mode filters. More recently, a non-conventional asymmetrical geometry for implementing mixed coupling between arbitrarily shaped coaxial resonators has been demonstrated in [25]. All the solution discussed so far, however, are based on three-dimensional (3-D) geometries of complex implementation.

It is also interesting to note that filter structures using mixed inductive and capacitive couplings to implement transmission zeros have also been proposed using standard PCB technology [26]-[29]. The structures proposed are indeed very compact and selective, however, the implementations reported are limited to one or two pole single (or double) pass band implementations.

In this context, therefore, we propose in this paper simple geometries to implement mixed couplings that can be easily manufactured. A preliminary implementation of this solution was recently discussed in [30], where a filter with TZs located above the pass-band was successfully demonstrated.

Manuscript received December 03, 2020; revised February 15, 2021; accepted March 19, 2021. Date of publication XXXXX XX 202x.

This work has been supported by the "Ministerio de Ciencia e Innovación" through the coordinated project PID2019-103982RB-C41.

J. J. Vague, D. Rubio, M. A. Fuentes, S. Cogollos, V. E. Boria, M. Baquero and M. Guglielmi are with Departamento de Comunicaciones, iTEAM, Universitat Politecnica de Valencia, E-46022, Spain (e-mails: jvague@dcom.upv.es, vboria@dcom.upv.es, marco.guglielmi@iteam.upv.es).

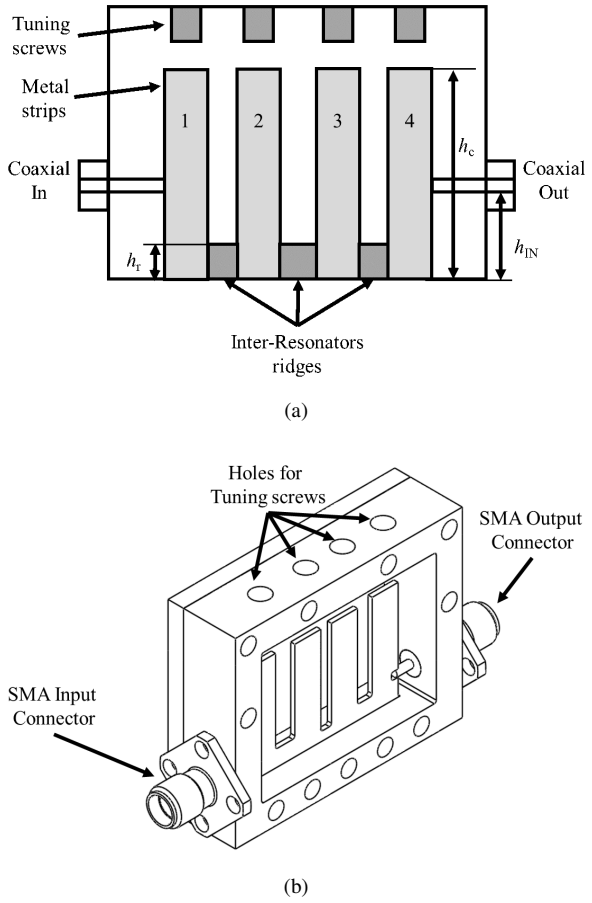

Fig. 1. Schematic of a longitudinal cut of the proposed combline filter composed of 4 resonators with mixed couplings in (a), and 3-D view of the complete filter structure in (b).

This paper is a substantially extended version of that previous work, where we show how a filter of order N can be used to implement N+1 TZs placed both below and (or) above the filter pass band. In addition, a low-cost fabrication technique based on Printed-Circuit Boards (PCBs) is also discussed. Furthermore, a systematic design procedure that allows for the independent control of the filter pass band and of the location of the TZs is fully described. In addition to theory, several prototypes are manufactured and measured showing very good agreement with simulations thereby fully validating the new filter concept.

II. Basic filter and Equivalent Circuit

The basic filter geometry that we propose in this paper is shown in Fig. 1. All resonators have a thickness of 0.8 mm, and a length of 5 mm. The complete filter is enclosed in a 25 mm by 10 mm rectangular metallic enclosure, as shown in Fig. 1.

One important point is that the couplings between adjacent resonators are implemented with sections of ridge waveguide (with height h_r as shown in Fig. 1). The inter resonator ridge waveguide sections operate below cut-off in the frequency range of the band pass response and, therefore, behave as series inductors [31].

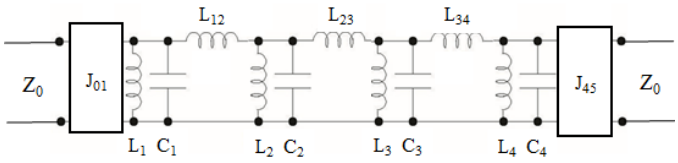

Fig. 2. Equivalent circuit of a combline bandpass filter of order N=4 using inductors as inter-resonator couplings.

The lumped element equivalent circuit for the basic filter is shown in Fig. 2. As we can see, the combline resonators are modeled with the parallel connection of an inductor (L_i) and a capacitor (C_i), as proposed in classical works [32]. The ridge waveguide section is modeled with a series inductor ($L_{i\ \ i+1}$). With our implementation, based on below cutoff ridge waveguide sections, the coupling level between adjacent resonators depends on two physical parameters, namely, the height of the ridge (h_r) and its length, that is, the separation between adjacent resonators. This choice provides an additional degree of freedom in the design process that will be exploited to control the location of the TZs.

III. Design Process

The filter examples discussed in this section are of order 4, have a pass band response centered at f_0 =3.85 GHz (S-band), and a bandwidth (BW) of 300 MHz (relative BW 7.8%). The starting point of the design process is a classical bandpass filter prototype composed of L-C resonators coupled through admittance inverters of suitable values [32]. The admittance inverters (except for the first and the last ones) are then replaced by an equivalent pi-network composed of three inductors [32]. After simple circuit manipulations, the corresponding equivalent circuit is shown in Fig. 2.

A. Resonator

As we can see in Fig. 2, the physical combline resonators are represented with a parallel resonant circuit. We will now describe how to find the L and C values. For this purpose, we first evaluate the input admittance Y_{0i}, looking from the bottom of the resonator toward the resonator open end, as discussed in [33]. This input admittance can be easily computed using available full-wave software tools (such as FEST3D v.2019 or CST Microwave Studio v.2019, Dassault Systèmes). Using the commercial tool CST Microwave Studio, we have then computed the resonance frequencies as a function of the height (h_c) of the metal strip. The results obtained are shown in Fig. 3. Moreover, the same full-wave software tool has provided a value of $Y_{0i} = \ 0.0121\ S$. For this classical resonator based on a coaxial line terminated with a capacitor, the following expression can then be used to find the slope parameter b_i of the resonator [32]

$$b_i\Big|_{i=1\ldots n} = Y_{0i}\left\{\frac{cot(\theta_0)+\theta_0 csc^2(\theta_0)}{2}\right\} \qquad (1)$$

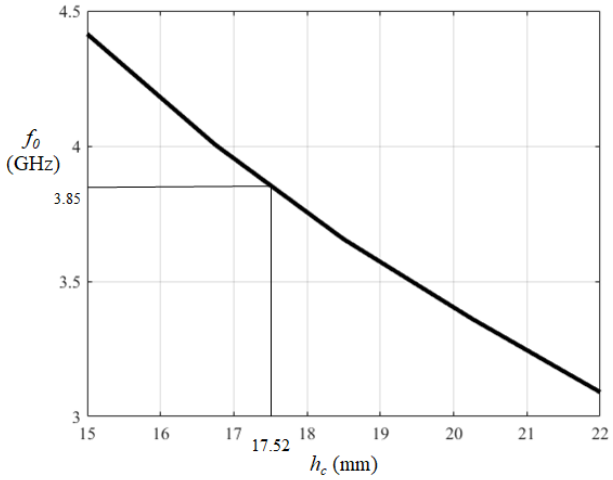

Fig. 3. Resonance frequency (in GHz) of the resonator of the combline filter in terms of the height h_c (in mm) of the metal strip in Fig. 1.

TABLE I
SCALED VALUES FOR THE EQUIVALENT CIRCUIT OF THE COMBLINE BANDPASS FILTER OF FIG. 2 (f_0 = 3.85 GHz AND RELATIVE BW 7.8 %)

Filter Element	Value
L_0	51.49 pH
C_0	33.19 pF
$J_{01} = J_{45}$	296.4 mS
$J_{12} = J_{34}$	67.70 mS
J_{23}	49.72 mS

where θ_0 is the electrical length (in radians) of the resonator at the centre frequency f_0 of the filter, which is easily computed as follows

$$\theta_0 = \frac{\omega_0}{c_0} h_c \tag{2}$$

where $\omega_0 = 2\pi f_0$, c_0 is the speed of light in free space, and h_c is the length of the coaxial transmission line. Once the resonance frequency f_0 and the corresponding slope parameter b_i of the real combline structure are known, we can compute the values (L_0 and C_0) of the equivalent L-C parallel resonant circuit with the following expressions

$$\omega_0{}^2 = (L_0 C_0)^{-1} \tag{3}$$

$$b_i = \omega_0 C_0 = (\omega_0 L_0)^{-1} \tag{4}$$

Following the procedure just outlined, we have then obtained the values of L_0 and C_0 shown in Table I. These values are scaled with respect to the characteristic admittance of the rectangular coaxial line Y_{0i} = 0.0121 S.

B. Admittance Inverter

Once the resonators have been modelled, the standard formulas from [32] are used to find the required values for all admittance inverters (collected again in Table I). To compute the values of the first and last inverters (J_{01} and J_{45}), we have assumed that the input/output ports have a normalized

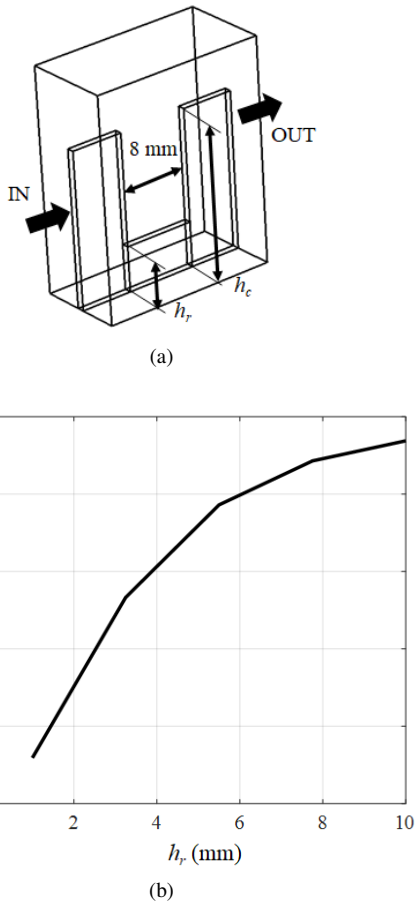

Fig. 4. Coupling provided by inter-resonator ridge waveguide sections (of length 8 mm and width 0.8 mm). In (a) simple 2-port structure, and in (b) magnitude of the S_{21} parameter (at f_0) for the structure shown in (a). The input and output ports of the structure are ridge waveguides of width 0.8 mm and height 17.52 mm.

characteristic impedance $\bar{Z}_0$ = 1 Ω ($\bar{Y}_0$ = 1 S). With this information, we can now easily compute the values of all coupling inductors in Fig. 2. We next use the inter-resonator ridge waveguide sections shown in Fig. 4 for the practical implementation of all inter-resonator coupling inductors. To this end, we fix the length of all the ridge waveguides to 8 mm, and we modify the height of the metal ridges (i.e. h_r in Fig. 1) to recover the requested coupling values between adjacent resonators. For this purpose, we have used the full-wave software tool FEST3D to compute the coupling level (magnitude of the S_{21} parameter) of the simple 2-port structure shown in Fig. 4. The results obtained for different values of h_r are shown in Fig. 4. Observing the results obtained, we can conclude that, as expected, the higher the metal ridge is, the higher the coupling value between resonators will be. A similar design curve can be obtained to relate the coupling level of the input and output coupling connections in terms of the physical parameter h_{IN} (see Fig. 1). The two design charts just described are very useful to define good initial solutions for the values of both h_r and h_{IN}, that are needed to implement the coupling levels of the corresponding inverters in the equivalent circuit representation of Fig. 2.

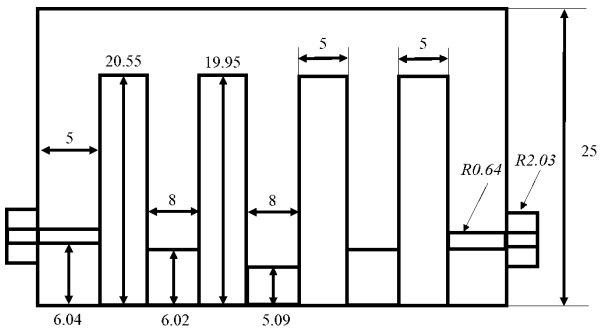

Fig. 5. Dimensions (in mm) of the 3-D geometry of the 4-pole combline filter with equivalent circuit elements collected in Table I. The dimensions not shown are inferred from symmetry.

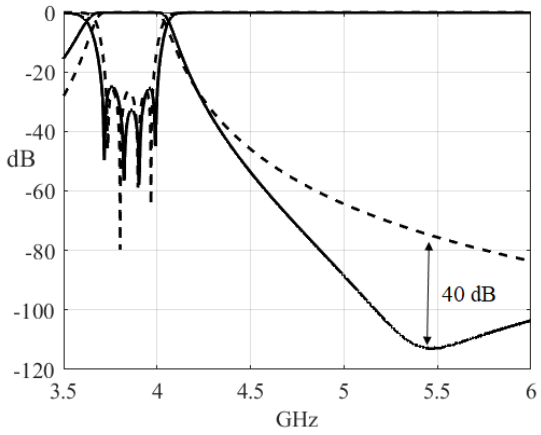

Fig. 6. S-parameters of the combline filter shown in Fig. 5. The simulated results obtained with FEST3D (solid lines) are compared with the results of the equivalent circuit in Fig. 2 (dotted lines).

C. Combline Filter

We can now proceed to complete the design procedure of the combline filter. All the variables that we need are defined in Fig. 5. As indicated before, the first step is to find the initial value for the heigth (h_c) of all resonators using Fig. 3. Then, we find new values for the height of each metal strip that is needed to recover the resonant frequency of each parallel resonator in the equivalent circuit of Fig. 2, from the available values of L_i and C_i, (with $i = 1, 2, 3, 4$). Note that the values of L_i and C_i are obtained from L_0 and C_0, after considering the loading effect due to the shunt elements of the equivalent circuits of the adjacent inverters. Next, for each inter resonator inductance L_{12}, L_{23} and L_{34} in the equivalent circuit in Fig. 2, we compute the related magnitude of the S_{21} parameter. We then use this value in the design chart of Fig. 4, thus obtaining the required value for the height of the corresponding inter-resonator ridge waveguide section.

A similar procedure is also followed to find the value for the geometrical parameter h_{IN} to recover the required input coupling level (J_{01} in the equivalent circuit) with the coaxial excitation (see Fig. 1). For this purpose, we use the design chart relating the coupling levels to h_{IN} . In this case, this chart has been computed considering a fixed length for the coaxial pin section of 5 mm. Due to symmetry, $J_{45} = J_{01}$, and therefore the same value of h_{IN} can be used for both coaxial input and output ports.

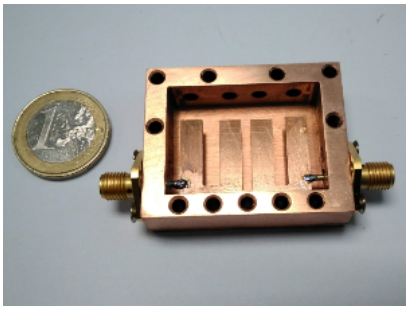

(a)

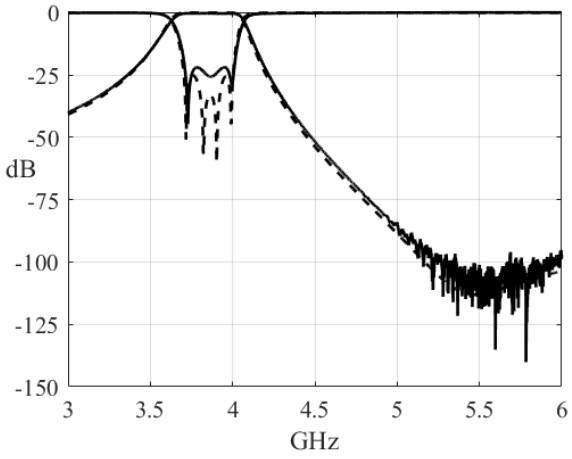

(b)

Fig. 7. Manufactured prototype of the combline filter in (a), and comparison of the measured results (solid lines) with the full-wave simulation data (dashed lines) in (b).

The procedure just described does provide a good set of initial values for the filter dimensions. A fine optimization process is, however, needed in order to obtain the desired bandpass response. The optimized final values for all geometrical variables of the filter are collected in Fig. 5. The full-wave simulated response of the filter obtained with FEST3D is shown in Fig. 6. The ElectroMagnetic (EM) simulation is compared with the response of the equivalent circuit of Fig. 2. Good agreement is shown in the pass band between both results, thus fully validating the proposed design procedure.

It is important to note, however, that there is a difference up to 40 dB in the IL values around 5.5 GHz. This difference has motivated further research in the behavior of the structure that we propose, as detailed in the next sections.

The combline filter just designed has also been manufactured using a low-cost fabrication technique, as shown in Fig. 7. Tuning screws have been used to compensate manufacturing errors. The comparison between measured and simulated data for this filter is also shown in Fig. 7. These measured results, as well as all others included in the remainder of this document, are obtained with a Vector Network Analyzer (VNA) Rohde-Schwarz model ZNB20-2Port, after performing the corresponding calibration procedure. A reasonably good

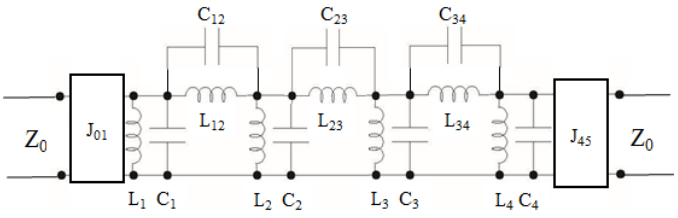

Fig. 8. Equivalent circuit of the combline filter with electric and magnetic inter-resonator couplings.

TABLE II
RESONANT FREQUENCIES AND SCALED L-C VALUES FOR THE EQUIVALENT CIRCUIT FIG. 8 OF THE FILTER STRUCTURE IN FIG. 10

Frequency	Value (GHz)	L - C (pH - fF)
f_1	3.4901	2371.0 - 887.1
f_2	3.6669	603.2 - 3123.0
f_3	3.6222	674.6 - 2862.0
f_4	3.5554	1780.0 - 1126.0
f_{12}	4.5500	2422.0 - 505.2
f_{23}	4.3700	1526.0 - 869.2
f_{34}	5.2850	4362.0 - 207.9

agreement for both S_{11} and S_{21} parameters has indeed been obtained both in-band and out-of-band. It is also important to note that a deep attenuation valley around 5.5 GHz is observed also in the measurements. This confirms the result predicted by the full-wave simulator.

IV. IMPLEMENTING TRANSMISSION ZEROS (TZS)

A. TZs above the passband

The magnetic coupling mechanism that is discussed in section III is not sufficient by itself to create TZs in the response of the filter. To implement TZs, as discussed in [23]-[25], we need to change the series inductances L_{12}, L_{23} and L_{34} of the equivalent circuit in Fig. 2 into resonant parallel L-C circuits. In physical terms this means that the resonators must be coupled both magnetically and electrically. We now show in Fig. 8 the modified equivalent circuit, where we have added to the inter-resonator couplings the capacitive couplings C_{12}, C_{23}, and C_{34}. The new parallel L-C combination now allows for the implementation of three (N-1) TZs for a filter of order four (N = 4). In particular, L_{12} and C_{12} are responsible for TZ_{12} at frequency f_{12}. The pair L_{23} and C_{23} is responsible for TZ_{23}. TZ_{34} at f_{34} is generated by L_{34} and C_{34}. From a physical point of view, this additional capacitive coupling is provided in the structure in Fig. 1 by the capacitive coupling that takes place naturally between the open-ended termination of the resonators, where the electric field is more intense.

The use of a capacitive coupling to create a TZ has already been discussed in the technical literature (see for instance [24]). However, in [24] the additional capacitive coupling is obtained adding a lumped element capacitor. This, in turn, introduces additional IL. In our case, we do not use any external element so that no additional losses are introduced. Furthermore, it is important to note at this point that the inductive coupling discussed in section III has also been discussed

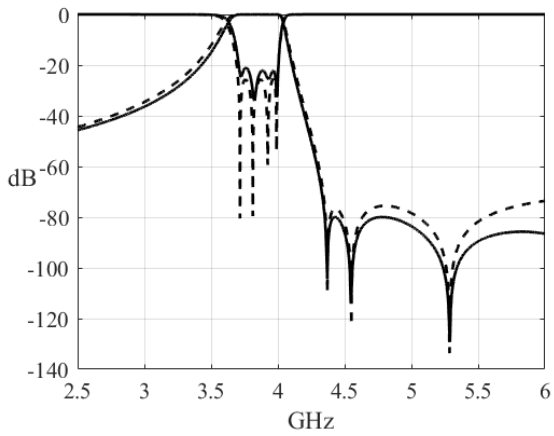

Fig. 9. Comparison of the frequency response obtained with FEST3D (continuous line) and the equivalent circuit (dotted line). The same TZ frequencies (at 4.37, 4.55 and 5.285 GHz) are evident in both responses.

already in the technical literature (see, for instance [14], [31]). However, the ridge coupling and the capacitive coupling have been used separately and not in conjunction as it is the case in this paper. This, together with the simplicity of the structure that we propose, are, in fact, two of the innovations that we discuss in this paper. With this understanding, we now realize that in the physical structure of the filter, we do have two degrees of freedom for the independent adjustment of both the L and the C for the inter resonator couplings. As already discussed, the height of the ridge waveguide can be used to adjust the value of L, while the distance between resonators can be used to adjust the value of C. The two parameters can, in fact, be used to implement, at the same time, the desired TZ, and the required coupling value. After that, the resonant inter-resonator elements are introduced maintaining, at the same time, the desired coupling levels and the TZ locations. We then have used an optimization process to recover the desired filter response including both pass band and TZ locations. Table II shows the various frequencies for the equivalent circuit in Fig. 8, and the corresponding L-C pairs scaled with respect to the characteristic admittance Y_{0i}.

It is important to mention, at this point, that it is indeed possible to obtain the values of the components of the equivalent circuit in Fig. 8 directly from the filter specifications as discussed, for instance, in [34] and [35]. This is indeed an important point that increases significantly the usefulness and range of applicability of the structures that we propose.

Once the equivalent circuit values have been obtained, they can be used to design a new combline filter with TZs. The software FEST3D has been used to obtain the dimensions of the structure. One again, the technique used is to match the IL of sections of the equivalent circuit (resonators, inter-resonators and input/output couplings) of Fig. 8 with their respective physical combline implementation. Naturally, the resonators are now tuned at different frequencies (f_1 to f_4 in Table II). The initial value of the height of each resonator can again be found using the chart in Fig. 3. Next inter-resonators sections are dimensioned matching, at the same time, coupling

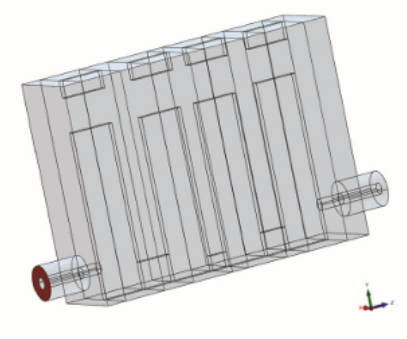

(a)

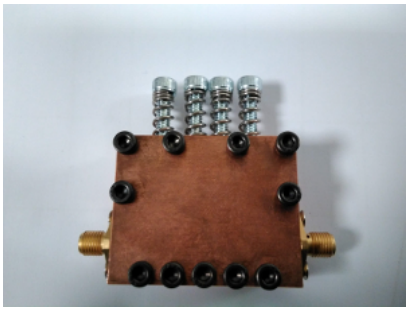

(b)

Fig. 10. Four-pole filter with TZs above the pass band. (a) Inner view designed with FEST3D. (b) Photograph of the manufactured prototype.

levels and TZs locations. After that, an optimization has been performed with FEST3D until the equivalent circuit and the simulated electric response of the combline filter are perfectly matched. The full-wave response of the filter simulated with FEST3D is shown in Fig. 9, where it is compared with the equivalent circuit results. The same TZ frequencies (at 4.37, 4.55 and 5.285 GHz) have indeed been obtained. There is only a small difference in the return loss levels. This discrepancy, however, is probably due the different wide band dispersive behaviour of the lumped element circuit and the EM simulator. We now show in Fig. 10 the structure of the combline filter with TZs. In the structure simulated, the tuning elements have been modeled with additional ridges near the top of the resonators. As we can see in Fig. 10, in the filter manufactured, the tuning ridges are replaced with standard screws. Fig. 11 shows the comparison of the simulated (FEST3D, dotted line) and the measured (continuous line) frequency response of the combline filter with TZs. Very good agreement is observed in the bandwidth, in the minimum return loss level, and in the location of the TZs in the upper rejection band. One interesting point is that we observe a total number of four TZs. Three of the TZs are due to the resonant inter-resonator coupling mechanism. Our investigations show that the fourth TZ near 6.5 GHz is due to a direct input-output coupling. This additional TZ does indeed help to extend the rejected band of the filter, but it cannot be easily controlled with the present configuration.

B. TZs below the pass band

In the previous section we discussed a combline filter with TZs above the pass band. In this section we will show how to

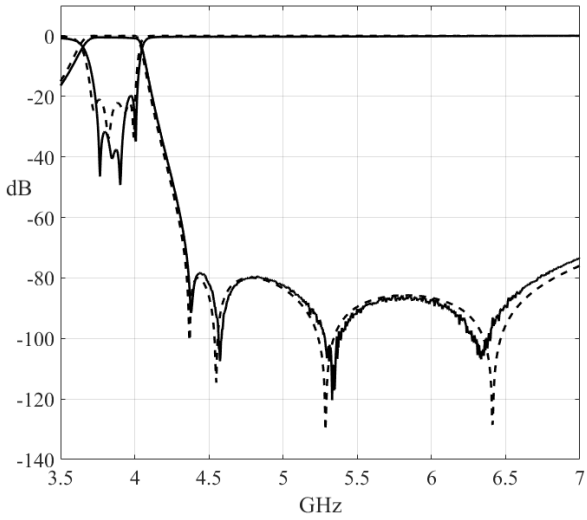

Fig. 11. Comparison of the measured (continuous line) and simulated (dotted line) performance of the combline filter with TZs.

TABLE III
RESONANT FREQUENCIES AND SCALED L-C VALUES FOR THE EQUIVALENT CIRCUIT (FIG. 8) OF THE FILTER STRUCTURE OF FIG. 12

Frequency	Value (GHz)	L - C (nH - fF)
f_1	3.5236	16.02 - 127.3
f_2	3.8733	3.68 - 458.3
f_3	3.8733	3.68 - 458.3
f_4	3.5236	16.02 - 127.3
f_{12}	5.7000	40.79 - 19.1
f_{23}	3.1400	24.92 - 103.1
f_{34}	6.1700	46.40 - 14.3

implement TZs below the pass band.

1) One TZ below: The equivalent circuit in Fig. 8 can also be used to design a filter with a TZ at a frequency that is below the filters pass band (Low-TZ filter). To achieve that, the corresponding inter-resonator L-C coupling must resonate below the pass band of the filter. If only one TZ is needed, the central inverter is the best place to introduce the resonant coupling (the pair $L_{23}-C_{23}$ in Fig. 8). In Fig. 12 we show the four-pole combline structure used to implement a low TZ. The structure needs a strong electric coupling between resonators 2 and 3, resulting in a greater value for C_{23} in the equivalent circuit of the filter of Fig. 8.

This filter has also been designed by matching the IL of each section of the filter with the corresponding section of the equivalent circuit. In Table III we show the resonant frequencies for the equivalent circuit of the Low-TZ filter. The values of all L-C pairs are scaled with respect to the characteristic impedance $Y_{0i} = \ 0.0121\ S$. The resonances f_1, f_2, f_3, and f_4 correspond to the resonators L_1-C_1, L_2-C_2, L_3-C_3 and L_4-C_4 in Fig. 8, respectively. Furthermore, the resonances f_{12}, f_{23}, and f_{34} correspond to the resonant pairs $L_{12}-C_{12}$, $L_{23}-C_{23}$, and $L_{34}-C_{34}$. They are the inter-resonators couplings that generate the TZs of the structure. In Table III we can see that the $L_{23}-C_{23}$ pair has the

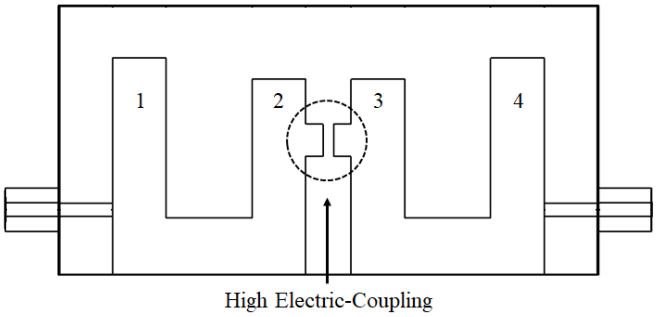

Fig. 12. Four-pole filter with TZ in the lower band. Note the presence of a strong electrical coupling mechanism between resonators 2 and 3.

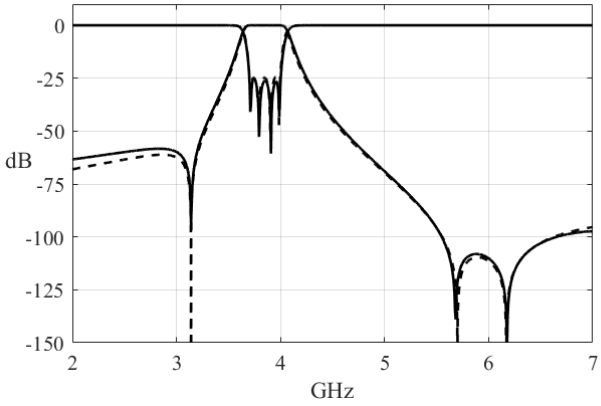

Fig. 13. Comparison of the frequency response obtained with the full-wave EM simulation of the combline filter (FEST3D: continuous line) and with the equivalent circuit model of Fig. 8 (dotted line).

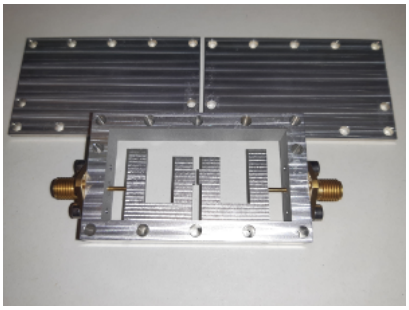

(a)

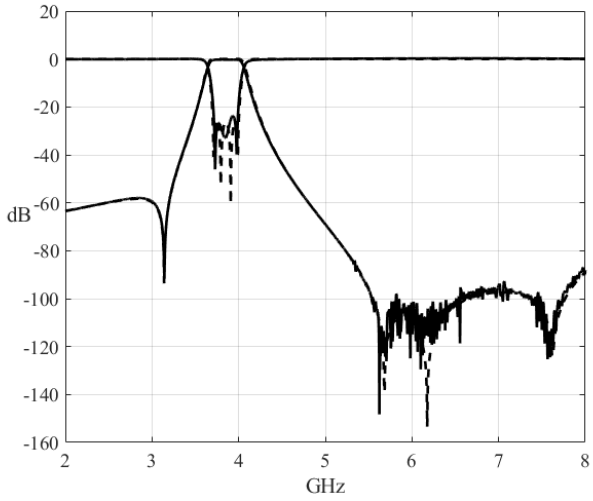

(b)

Fig. 14. In (a) the manufactured Low-TZ combline filter. In (b) comparison of the frequency response obtained with FEST3D (dotted line) and the measured response (continuous line).

largest capacitor of the three inter-resonator L-C pairs. This is reflected in a strong electric coupling mechanism in the central section of the Low-TZ filter (see Fig. 12).

As we can see in Fig. 13, we have achieved a very good agreement between the frequency response obtained with the L-C equivalent circuit of Fig. 8 and the filter structure simulated with FEST3D. Note that the filter has two more TZs above the pass band located at 5.70 and 6.17 GHz caused by the inter-resonators 1-2 and 3-4. In Fig. 14 the Low-TZ filter that we have manufactured in aluminium, using Wire Electrical Discharge Machining (WEDM) with a wire diameter of 0.8 mm, can be seen. In Fig. 14 we also show a comparison between the frequency response of the full-wave EM simulations (dotted line) and the measured filter response (continuous line). At 3.85 GHz (the central frequency of the prototype filter response) the measured value of the IL is 0.27 dB. Note that a third TZ is present at approximately 7.50 GHz. As already discussed, this TZ is due to a direct coupling between input and output ports. As we can see, there are indeed small discrepancies, probably due to manufacturing inaccuracies, both in terms of bandwidth and return loss level as compared to the ideal performance. On the other hand, an excellent agreement of the frequencies of the TZs has been clearly obtained. Thus, the design process and the basic filter features have been clearly validated.

2) Out of band performance: One aspect of the performance of any filter that is generally very important, is the out of band performance, both below and above the filter pass band. Naturally, moving the location of TZs from one side to the other of the filter pass band has a profound effect on the rejection levels. To illustrate this point, we show in Fig. 15 the simulated response of three different structures with identical pass band, namely, the filter in Fig. 7, the one in Fig. 10, and another filter structure with three TZs below the pass band. As we can see, the filter in Fig. 7 and the one in Fig. 10 have comparable rejection levels both above and below the pass band. The structure with three TZs below the pass band, however, has, as expected, a much better rejection level below the pass band, and substantially lower rejection level above the pass band. One issue that is important to note at this point is that the S_{21} curve with points and dashed lines in Fig. 15 has been obtained with a structure similar to the one in Fig. 12, but where all inter resonator couplings are resonant below the pass-band. Although it is indeed possible to simulate the resulting structure, the geometrical values of the capacitive gaps turn out to be too small for a practical implementation. This structure is, therefore, not discussed in this paper. A more practical solution to implement three TZs below the pass band is discussed in the next section.

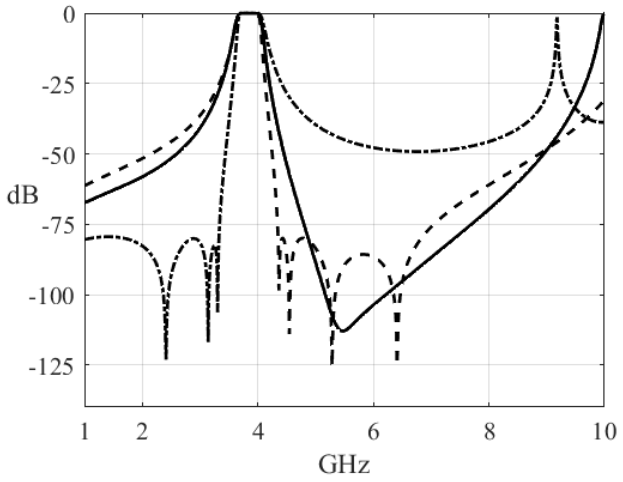

Fig. 15. Out of band performance of three different filters. The simulated results of S_{21} are shown with solid and dashed lines for the filters of Figs. 7 and 10, respectively, and with points and dashed lines for another filter with three TZs below the pass-band.

3) Three TZs below: The next application example that we describe is a filter with all 3 TZs in the lower band (Fig. 16). All the designs showed so far have been implemented in planar technology in air. The implementation we are now going to discuss makes use of a low cost Printed Circuit Board (PCB) with a dielectric substrate. The reason for this change is that to move all the TZs below the pass band requires significantly stronger capacitive couplings. This is much easier to implement using a dielectric substrate.

The PCB filter in Fig. 16 is again of order four. However, the center frequency is now 1.5 GHz, and the bandwidth is 300 MHz (20%). The resonators are now formed with two metallic strips in the opposite sides of a standard FR4 PCB (thickness of 1.6 mm, permittivity $\varepsilon_r = 4.4$ and $\tan(\delta) = 0.02$). In addition, they are inter-connected with soldered metal pins near the edges of the metal strips. The base of the PCB is soldered to the lower wall of the metallic enclosure. Input and output ports are standard SMA connectors. Their central pins are soldered to microstrip lines that connect to the first and last resonator, respectively. Even though the manufacturing technique is different, the principle of operation is the same as all the other examples discussed. In the upper wall of the metallic enclosure, we have included four tuning screws to tune the resonators. It is important to note the presence of a small ridge with $h_r = 1.5$ mm to implement the inductive component of the inter-resonator couplings. The electric component of the couplings is now significantly stronger due to the presence of the dielectric. Small gaps are implemented between metal posts (see Fig. 16) to locate the TZs below the pass band. The filter design procedure is identical to what we already discussed in section IV. Table IV shows values needed for a Chebyshev filter of order four, with 22 dB of return losses. The values are scaled with respect to the characteristic impedance of the coaxial resonator section (in this case, $Y_{0i} = 0.01525$ S), the normalized impedance of the input/output sections of the filter is $\bar{Z}_0 = 1$. The equivalent circuit of the PCB filter is

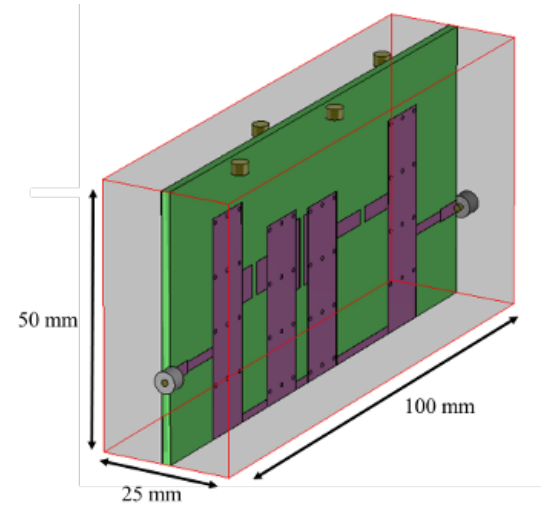

(a)

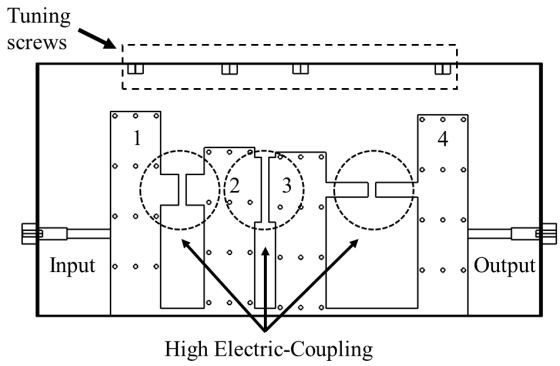

(b)

Fig. 16. Four-pole filter with three TZs in the lower band. Note the presence of a high electrical coupling mechanism between resonators 1-2, 2-3 and 3-4. In (a) 3D-view, and side view in (b).

TABLE IV
SCALED VALUES OF A BANDPASS FILTER CENTERED AT 1.5 GHZ, AND WITH A RELATIVE BW OF 20%

Filter Element	Value
L_0	646 pH
C_0	17.40 pF
$J_{01} = J_{45}$	195.9 mS
$J_{12} = J_{34}$	31.47 mS
J_{23}	23.83 mS

exactly the same as the one showed in Fig. 8. Table V shows the resonant frequencies (L-C pairs of Fig. 8) for the case in which all three TZs are below the pass band. In this case, the L-C values shown in Table V are also scaled with respect to the characteristic impedance Y_{0i} = 0.0152 S of Table IV. For this example, CST Microwave Studio has been used to include the presence of the dielectric substrate in all design phases. Fig. 17 shows the comparison between the response obtained with the equivalent circuit and the one of the PCB filter simulated with CST Microwave Studio. Note that the low-band TZs are located at 0.8, 1.12 and 1.3 GHz, respectively.

In Fig. 18 we show the PCB filter with the three TZs below

TABLE V
RESONANT FREQUENCIES AND SCALED L-C VALUES FOR THE EQUIVALENT CIRCUIT (FIG. 8) OF THE FILTER STRUCTURE IN FIG. 16

Frequency	Value (GHz)	L - C (pH - fF)
f_1	1.5554	2.66-3.94
f_2	1.8227	4.12-1.85
f_3	1.6625	2.44-3.76
f_4	1.5743	3.44-2.97
f_{12}	1.1200	16.26-1.25
f_{23}	0.8000	0.94-42.09
f_{34}	1.3000	5.03-3.09

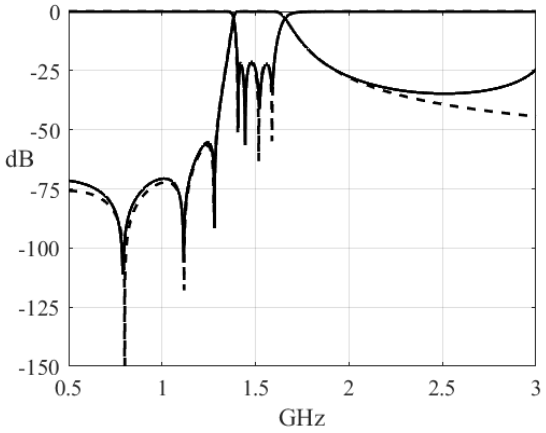

Fig. 17. Comparison of the frequency response of the combline filter shown in Fig. 16, obtained with CST Microwave Studio (continuous line) and with the equivalent circuit model of Fig.8 (dotted line).

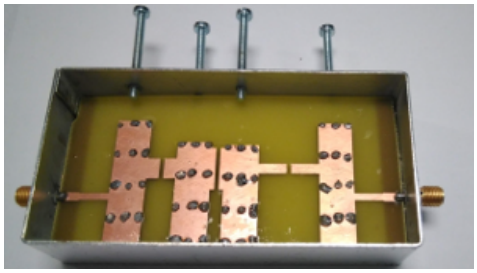

(a)

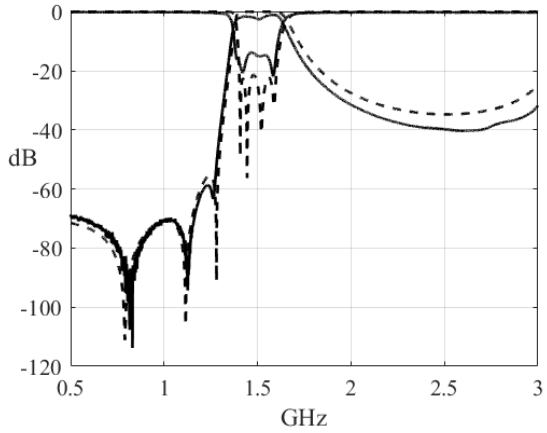

(b)

Fig. 18. Prototype of the combline filter with three TZs below tha pass-band in (a), and comparison between simulated (dotted lines) and measured (continuous lines) responses in (b).

the pass band, including the tuning screws, that has been manufactured in our in-house facility. This figure also shows the comparison between the frequency response obtained with CST Microwave Studio (dotted line) without losses, and the measured filter response (continuous line). A reasonable agreement is clearly shown for the location of the TZs. The PCB filter has a minimum return loss value of 14 dB instead of the 22 dB achieved in simulation. Up to 1.5 dB of IL can be seen in the pass band, mainly due to the lossy dielectric material. The manufacturing accuracy of the filter is rather low. As a consequence, the four tuning screws in the resonators are not sufficient to recover perfectly the simulated response. On the other hand, the design objective has been fully achieved, namely, the design of a PCB combline filter of order four with three TZs below the filter pass band.

V. TWO MORE TZS

All the filter structures that we have discussed so far can be used to introduce TZs using resonant inter-resonator couplings. The result is that with a filter of order N we can implement N-1 TZs. However, all the filters discussed have also two additional couplings, namely, the input and the output couplings. The objective of this section is, therefore, to show how the PCB structure in Fig. 16 can be easily modified to introduce resonant input and output couplings, so that two additional TZs can be implemented.

Fig. 19 shows a PCB filter, manufactured with a standard photo-lithographic process, on an FR-4 substrate. The central frequency is now 1.5 GHz and relative BW is 13%. The key feature of the design is the presence of an inductive coupling in parallel with a capacitive coupling to implement the input/output couplings. In Fig. 19 we can clearly see the spirals that implement the inductive element of the input/output couplings. The capacitive element of the input/output coupling is implemented with the section of the spiral that is parallel to the resonators. It is important to note that the additional resonant couplings are introduced without using external elements. Furthermore, the input/output couplings are the strongest ones in the whole filter structure, so that the additional capacitance and inductance do not introduce significant additional losses. Fig. 19 shows the frequency response of the filter. The IL is, again, approximately equal to 1.5 dB (FR-4 substrate). It is also important to mention that, because of the symmetry of the circuit, the two extra TZs are located in the same frequency, close to 800 MHz. The small differences observed between measurements (in continuous line) and simulations (in dotted line) are mainly due to the losses in the filter, and to the limited manufacturing accuracy. The measured value of IL can be mainly attributed to the low performance of the employed substrate material, as well as to the additional contribution of the practical realization of input/output couplings using the proposed quasi-lumped elements.

To continue, we now show in Fig. 20 a new design manufactured with the high performance RO-4003c substrate. The

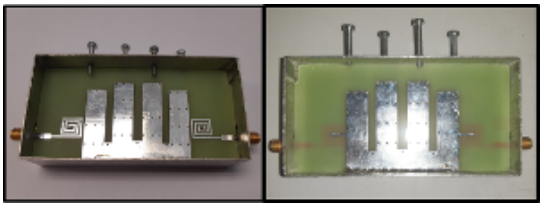

(a)

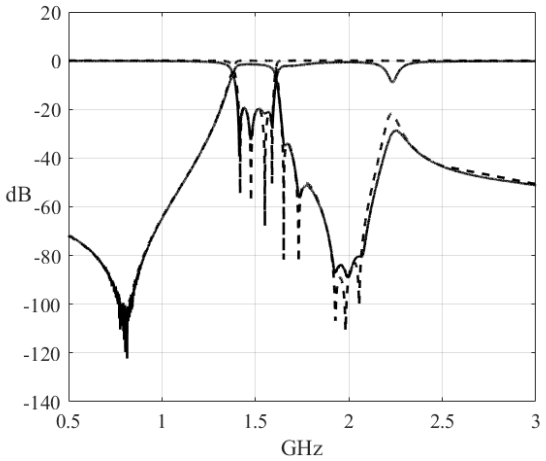

(b)

Fig. 19. Prototype of a combline filter with 2 joint TZs (from input/output couplings) implemented with an FR-4 substrate in (a), and comparison of the measured results, solid lines in (b), with the full-wave simulation data (dashed lines).

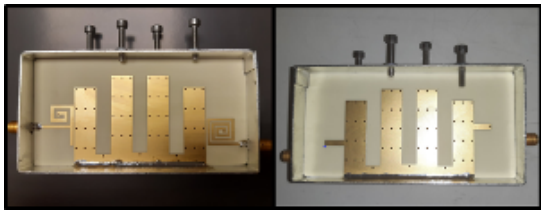

(a)

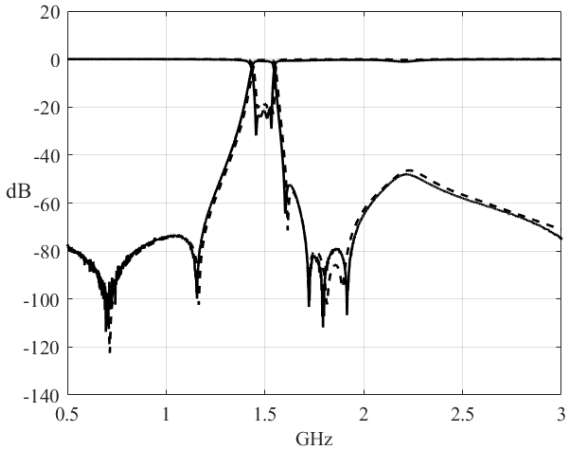

(b)

Fig. 20. Prototype of a combline filter with two separate TZs (from input/output couplings) implemented with an RO-4003c substrate in (a), and comparison of the measured results, solid lines in (b), with the full-wave simulation data (dashed lines).

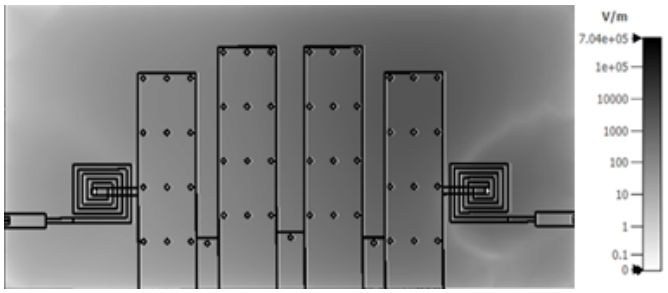

Fig. 21. Magnitude of the electric field in the filter prototype of Fig.19 (including the metal enclosure).

bandpass filter has the central frequency equal to 1.5 GHz and a relative BW of 6.7 %. The measured value of the IL of the filter prototype is less than 0.85 dB. Asymmetric input/output sections have been used now in order to obtain two separate TZs near 0.7 and 1.2 GHz, respectively, to the left of the passband of the filter. Up to five TZ are observed in the right side of Fig. 19. Three of them are due to the inter-resonator resonances. The periodic nature of the response of the spiral inductors implemented in the PCB introduces two additionally TZs in the high frequency region. Note that a similar phenomenon occurs in the filter of Fig. 20, but the fifth TZ is out of the measurement range showed in the figure.
Finally, the out-of-band responses of the last two filters is also included in Figs 19 and 20. As can be seen in both, there is a spurious peak around 2.20 GHz (of higher intensity in Fig. 19). A more detailed analysis using full-wave simulations indicates that these peaks are related to the excitation of a resonance of the metallic enclosures (as can be seen with the electric field results shown in Fig.21).

VI. Conclusions

In this article, we have extended the state-of-the-art of combline filters by discussing a new family of structures that can be used to implement up to N+1 transmission zeros with a simple in-line implementation of order N. Simple modifications of the classic combline filter structure have been shown to be very effective in the implementation and control of the position of N+1 TZs, in a filter of order N. The presence of the TZs has been explained in terms of mixed electric and magnetic couplings. A systematic design procedure has also been fully discussed. In addition to theory, two different implementations (in L- and S-bands) have been used to verify the novel filter topologies. Finally, the experimental validation of all the designs has been performed. Good agreement between simulations and measurements has been shown in all cases, thereby fully validating the new family of filter structures.

References

[1] R.J. Cameron, C.M. Kudsia and R.R. Mansour, *Microwaves Filter for Communications Systems: Fundamentals, Design and Applications,* Hoboken, NJ, USA: Wiley, 2nd ed., 2018.
[2] G.L. Matthaei, "Comb-line band-pass filters of narrow or moderate bandwidth", *Microw. J.,* vol.6, pp. 82-91, Aug. 1963.
[3] E.G. Cristal, "Tapped-line coupled transmission lines with applications to combline and interdigital filters", *IEEE MTT-S Int. Microw. Symp.,* Palo Alto, CA, pp. 110-112, 1975.

[4] G.L. Matthaei, "Interdigital band-pass filters", *IRE Trans. Microw. Theory Tech.,* pp. 479-491, Nov. 1962.

[5] R.M. Kurzrok, "Design of comb-Line band-pass filters", *IEEE Trans. Microw. Theory Tech.,* pp. 351-353, Jul. 1966.

[6] J.D. Rhodes, "The stepped digital elliptic filters", *IEEE Trans. Microw. Theory Tech.,* vol. , no 4, pp 178-184, Apr. 1969.

[7] J.D. Rhodes, "The theory of generalized interdigital networks", *IEEE Trans. Circuit Theory,* vol. CT-16, No 3, pp. 280-288, Aug. 1969.

[8] R. Levy and J.D. Rhodes, "A comb line elliptic filter", *IEEE Trans. Microw. Theory Tech.,* vol. 19, no 1, pp. 26-29, Jan. 1971.

[9] R.J. Wenzel, "Synthesis of combline and capacitively loaded interdigital bandpass filters of arbitrary bandwidth", *IEEE Trans. Microw. Theory Tech.,* vol. 19, no. 8, pp. 678-687, Aug. 1971.

[10] I.H. Zabalawi, "Design of linear phase selective comb-line filter", *IEEE Trans. Microw. Theory Tech.,* vol. 30, no. 8, pp. 1224-1229, Aug. 1982.

[11] A. Morini, G. Venanzoni, and T. Rozzi, "A new adaptive prototype for the design of side-coupled coaxial filters with close correspondence to the physical structure", *IEEE Trans. Microw. Theory Tech.,* vol. 54, no. 3, pp. 1146-1153, Mar. 2006.

[12] H. W. Yao, K. A. Zaki, A. E. Atia, and R. Hershtig "Full wave modelling of conducting posts in rectangular waveguides and its application to slot coupled combline filters", *IEEE Trans. Microw. Theory Tech.,* vol. 43, no. 12, pp. 2824–2830, Dec. 1995.

[13] R. J. Cameron, "General coupling matrix synthesis methods for Chebyshev filtering functions", *IEEE Trans. Microw. Theory Tech.,* vol. 47, no. 4, pp. 433-442, Apr. 1999.

[14] J.M. Peters, "Resonant coupling elements" US Patent No.: 6611183 B1, Aug. 26, 2003.

[15] J.B. Thomas, "Cross-coupling in coaxial cavity filters - a tutorial overview", *IEEE Trans. Microw. Theory Tech.,* vol. 51, no. 4, pp. 1368–1376, Apr. 2003.

[16] S. Shin, R.V. Snyder, "At least N+1 finite transmission zeros using frequency-variant negative source-load coupling", *IEEE Microw. and Wireless Components Letters,* vol. 13, no. 3, pp. 117-119, Mar. 2003.

[17] J. R. Rhodes, R. J. Cameron, "General extracted pole synthesis technique with application to low-loss TE011-mode filters", *IEEE Trans. Microw. Theory Tech.,* vol. 28, no. 9, pp. 1018-1028, Sep. 1980.

[18] S. Amari, G. Macchiarella, "Synthesis of inline filters with arbitrarily placed attenuation poles by using nonresonating nodes", *IEEE Trans. Microw. Theory Tech.,* vol. 53, no. 10, pp. 3075-3081, Oct. 2005.

[19] S. Cogollos, R.J. Cameron, R.R. Mansour, M. Yu, V.E. Boria, "Synthesis and design procedure for high performance waveguide filters based on nonresonating nodes", *IEEE MTT-S Int. Microw. Symp. Dig.,* pp. 1297-1300, Jun. 2007.

[20] G. Macchiarella, M. Fumagalli, "Inline comb filters with one or two transmission zeros", *IEEE MTT-S Int. Microw. Symp. Dig.,* vol. 2, pp. 1085-1088, Oct. 2004.

[21] Y. Wang, M. Yu, "Inline realization of cascaded trisection and cascaded quadruplet in coaxial cavity filters", *Proc. of the 2009 European Microw. Conf. (EuMC),* pp. 448-451, Oct. 2009.

[22] M. Hoft, F. Yousif, "Orthogonal coaxial cavity filters with distributed cross-coupling", *IEEE Microw. and Wireless Components Letters,* vol. 21, Issue: 10, pp. 519-521, Aug. 2011.

[23] H. Wang, Q.X. Chu, "An inline coaxial quasi-elliptic filter with controllable mixed electric and magnetic coupling", *IEEE Trans. Microw. Theory Tech.,* vol. 57, no. 3, pp. 667-673, Feb. 2009.

[24] S. Bastioli, R.V. Snyder and P. Jojic, "High power in-line pseudoelliptic evanescent mode filter using series lumped capacitors," *2011 41st European Microw. Conf.,* Manchester, pp. 87-90, Oct. 2011.

[25] G. Venanzoni, M. Dionigi, C. Tomassoni and R. Sorrentino, "3-D-printed quasi-elliptical evanescent mode filter using mixed electromagnetic coupling," *IEEE Microw. and Wireless Components Letters,* vol. 28, no. 6, pp. 497-499, Jun. 2018.

[26] T. Yan, D. Lu, J. Wang and X. Tang, "High-selectivity balanced bandpass filter with mixed electric and magnetic coupling," *IEEE Microw. and Wireless Components Letters,* vol. 26, no. 6, pp. 398-400, Jun. 2016.

[27] Z. Cai, X. Tang, Z. Li, T. Zhang, Y. Liu and Y. Yang, "A low phase noise differential oscillator employing stub-loaded nested split-ring resonator inspired balanced bandpass filter," *2019 IEEE MTT-S Int. Microw. Symp. (IMS),* Boston, MA, USA, pp. 967-970, May 2019.

[28] Z. Cai, Y. Liu, X. Tang and T. Zhang, "A novel low phase noise oscillator Using Stubs Loaded Nested Split-Ring Resonator," *IEEE Microw. and Wireless Components Letters,* vol. 27, no. 4, pp. 386-388, Apr. 2017.

[29] P. Wen, Z. Ma, H. Liu, M. Ohira, B. Ren and X. Wang, "Compact dual-band bandpass filter using stub-loaded stepped impedance resonators with mixed electric and magnetic couplings," *2017 IEEE Asia Pacific Microw. Conf. (APMC)*, Kuala Lumpur, pp. 803-805, Nov. 2017.

[30] J. Vague, J. Ossorio, S. Cogollos, V.E. Boria, M. Guglielmi, "Optimized design of combline filters with transmission zeros," *2019 IEEE MTT-S Int. Conf. on Numerical Electromagnetic and Multiphysics Modeling and Optimization (NEMO),* Boston, USA, pp. 1-4, May 2019.

[31] R.V. Snyder, S. Bastioli, "Broad passband, wide stopband, high power evanescent mode filters using capacitively-loaded ridges ", *2012 42nd European Microw. Conf.*, Amsterdam, The Netherlands, pp. 176-179 , Oct 2012.

[32] G. Matthaei, L. Young, E.M.T. Jones, *Microwave Filters Impedance Matching Networks and Coupling Structures,* Norwood, MA. USA: Artech House Inc., 1980.

[33] E. Tarín, P. Soto and V.E. Boria, "Accurate modal representation of arbitrarily shaped multiconductor transmission lines enclosed in homogeneous waveguides," *IEEE MTT-S Int. Microw. Symp. Dig.,* Long Beach, CA, USA, pp. 1067-1070, Jun. 2005.

[34] S. Tamiazzo and G. Macchiarella, "Synthesis of cross-coupled filters with frequency-dependent couplings",*Trans. Microw. Theory Tech.,* vol. 65, no. 3, pp. 775–782, Mar. 2017.

[35] Y. He et al., "A direct matrix synthesis for in-line filters with transmission zeros generated by frequency-variant couplings", *IEEE Trans. Microw. Theory Tech.,* vol. 66, no. 4, pp. 1780–1789, Apr. 2018.